JGR Oceans

RESEARCH ARTICLE
10.1029/2019JC015072

Special Section:
Midlatitude Marine Heatwaves: Forcing and Impacts

Formation, Development, and Propagation of a Rare Coastal Coccolithophore Bloom

Paul G. Matson[1,2], Libe Washburn[3], Erik A. Fields[4], Chris Gotschalk[1], Tanika M. Ladd[5], David A. Siegel[3,4], Zoë S. Welch[5], and M. Debora Iglesias-Rodriguez[5]

[1]Marine Science Institute, University of California, Santa Barbara, Santa Barbara, CA, USA, [2]Now at Department of Biological Sciences, Bowling Green State University, Bowling Green, OH, USA, [3]Department of Geography, University of California, Santa Barbara, Santa Barbara, CA, USA, [4]Earth Research Institute, University of California, Santa Barbara, Santa Barbara, CA, USA, [5]Department of Ecology, Evolution, and Marine Biology, University of California, Santa Barbara, CA, USA

Abstract This study examines an unprecedented bloom of *Emiliania huxleyi* along the California coast during the NE Pacific warm anomaly of 2014–2015. Observations of coccolithophore populations from microscopy and flow cytometry, surface current data derived from high-frequency radar, and satellite ocean color imagery were used to track the population dynamics of the bloom in the Santa Barbara Channel. Results show a coastal bloom of mostly *E. huxleyi* that reached cell concentrations up to 5.7×10^6 cells per liter and a maximum spatial extent of 1,220 km^2. We speculate that the rare cooccurrence of warm water, high water column stability, and an extensive preceding diatom bloom during the anomaly contributed to the development of this bloom. Flow cytometry measurements provided insight on the phases of bloom development (e.g., growth versus senescence) with calcified cells comprising up to 64% of particles containing chlorophyll a and detached-coccolith:cell ratios ranging from 10 to >100. Lagrangian particle trajectories estimated during two nonoverlapping 48- and 72-hr periods showed the changes in the surface structure of the bloom due to advection by surface currents and nonconservative biological and physical processes. Time rates of change of particulate inorganic carbon were estimated along particle trajectories, with rates ranging from −4 to 6 μmol·L^{-1}·day^{-1}. The approach presented here is likely to be useful for understanding the evolution of coastal phytoplankton bloom events in a general setting.

Plain Language Summary This study examines an unprecedented bloom of the coccolithophore *Emiliania huxleyi*, a single-celled algae that is covered by calcium carbonate plates, along the California coast during a period of unusually warm water during 2014–2015. We used microscopy and flow cytometry, surface current data, and satellite ocean color imagery to track how the bloom changed through time in the Santa Barbara Channel. Results show a coastal bloom of mostly *E. huxleyi* that reached cell concentrations up to 5.7×10^6 cells per liter and covered up to 1,220 km^2. We speculate that the rare cooccurrence of environmental conditions, including warm water, high water column stability, and an extensive preceding diatom bloom during the anomaly, contributed to the development of this bloom. Flow cytometry measurements provided insight on the phases of bloom development (e.g., growth versus senescence) and hourly surface current data to simulate how currents may have moved the coccolithophores during the course of the bloom. In addition, we combined this data with satellite imagery to estimate how the amount of calcium carbonate in this bloom changed through time. The approach presented here is likely to be useful for understanding the rise and fall of phytoplankton blooms along the coast.

Key Points:
- Unprecedented coastal bloom of the coccolithophore *Emiliania huxleyi* during 2014/2015 warming anomaly occurring along the California coast
- Lagrangian particle trajectories showed changes in bloom structure due to advection by surface currents and nonconservative processes
- Bloom phases identified based on particle trajectories and satellite-derived estimates of change in particulate inorganic carbon

Supporting Information:
- Supporting Information S1

Correspondence to:
P. G. Matson,
pmatson@gmail.com

Citation:
Matson, P. G., Washburn, L., Fields, E. A., Gotschalk, C., Ladd, T. M., Siegel, D. A., et al (2019). Formation, development, and propagation of a rare coastal coccolithophore bloom. *Journal of Geophysical Research: Oceans*, *124*, 3298–3316. https://doi.org/10.1029/2019JC015072

Received 18 FEB 2019
Accepted 20 APR 2019
Accepted article online 29 APR 2019
Published online 22 MAY 2019

1. Introduction

The NE Pacific warm anomaly of 2014–2015, commonly referred to as "the Blob," brought about unprecedented changes in the oceanographic environment along the west coast of the North America. During this large-scale event, sea surface temperature anomalies of up to +5 °C were observed along the California coast (Bond et al., 2015; Reed et al., 2016). This was followed by an El Niño event beginning in early spring of 2015 (Leising et al., 2015; McClatchie et al., 2016), thus extending the period when California's coastal marine ecosystems experienced unusually warm temperatures. Following a widespread diatom bloom of *Pseudo-nitzschia* spp. along the U.S. West Coast (McCabe et al., 2016), an unprecedented

coccolithophore bloom was observed within the Santa Barbara Channel (SBC) in May and June of 2015 (http://www.news.ucsb.edu/2015/015490/living-color). The bloom turned the ocean surface turquoise in color, similar to the color of offshore coccolithophore blooms observed in the open ocean at higher latitudes (Balch et al., 1991; Holligan et al., 1983).

Coccolithophores are a widespread group of nanoplanktonic algae that typically bloom seasonally in both offshore and coastal waters and constitute an important component of the marine carbon system via their production of calcium carbonate (Heimdal et al., 1994; Holligan et al., 1993). Over the past few decades, coccolithophore abundances in the North Atlantic Ocean have increased along with rising ocean CO_2 concentrations and temperature (Rivero-Calle et al., 2015) making coccolithophores a potential sentinel species for marine ecosystems impacted by climate change. *Emiliania huxleyi* is often observed within the California Current System (Venrick, 2002, 2015) but has not previously been found reaching bloom cell concentrations (Winter, 1985; Ziveri et al., 1995), defined by Tyrrell and Merico (2004) as concentrations exceeding 10^6 cells per liter.

Blooms of *E. huxleyi* typically occur in ocean environments with high stratification, high light levels, and semioligotrophic conditions (Iglesias-Rodriguez et al., 2002; Tyrrell & Merico, 2004). Blooms are generally observed within shallow surface mixed layers (10–20 m deep), where *E. huxleyi* thrives since it does not exhibit photoinhibition at light levels of at least 1,500 μmol photons·m^{-2}·s^{-1} depending on the strain (Balch et al., 1992; Nanninga & Tyrrell, 1996). Blooms of *E. huxleyi* often follow diatom blooms in conditions of relatively reduced nitrate concentrations (Iglesias-Rodriguez et al., 2002). Although less competitive for nutrients than larger diatoms under replete conditions, *E. huxleyi* possesses highly efficient mechanisms for nutrient uptake when nutrient concentrations are low as it can utilize both inorganic and organic forms of nitrogen and phosphorus and has low requirements for iron and other micronutrients (Benner & Passow, 2010; Riegman et al., 2000).

Large blooms of *E. huxleyi* are easily identified via ocean color satellite remote sensing due to the high reflectance of coccoliths, the calcium carbonate plates surrounding the cells that are shed during cell division (Ackleson et al., 1994; Balch et al., 1991; Holligan et al., 1993). These plates contribute to particulate inorganic carbon (PIC), which is an important indicator of cell concentration and the growth stage of the bloom. For example, the ratio of detached coccoliths to cells increases with bloom age (Balch et al., 1996) and is governed by nutrient and light availability (Müller et al., 2008; Paasche, 2002), with sharp increases in coccolith detachment rates during nutrient and light stress (Paasche, 2002). However, because reflectance-based observations detect coccoliths in surface waters that are shed from cells over time as the population develops, satellite observations are unable to detect early bloom development. Instead, initial satellite detection is typically at the beginning of the populations' stationary growth phase when shed coccoliths are abundant and waters have been largely depleted of nutrients by the developing bloom (Balch et al., 1993; Balch et al., 1996; Holligan et al., 1993). Additionally, satellite studies of coastal phytoplankton dynamics are often limited by cloud cover or suspended sediments obscuring the blooms (Henderikx Freitas et al., 2017; Tyrrell & Merico, 2004).

A few recent studies have employed remote sensing and model determinations of surface velocities to interpret the evolution of coastal phytoplankton blooms. For example, Jönsson et al. (2009) presented a Lagrangian method for integrating satellite observations with an operational ocean circulation model to assess changes in water parcels through time. The authors have subsequently applied this approach to estimate rates of net phytoplankton production in the Gulf of Maine (Jönsson et al., 2011) and in the Southern California Bight (Jönsson & Salisbury, 2016). Similar approaches have been used to model the likelihood and advection of harmful algal blooms along the California coast (Anderson et al., 2016) and in Lake Erie (Rowe et al., 2016; Wynne et al., 2011, 2013).

Here we applied a method combining satellite ocean color imagery, in situ sampling, and surface current observations from high-frequency (HF) radars to examine the formation and evolution of the *E. huxleyi* bloom that occurred in the SBC in June 2015. Unlike blooms of other phytoplankton, blooms of *E. huxleyi* remain near the surface (see review by Zondervan, 2007) where HF radars provide information on the changing current patterns that influence their spatial and temporal evolution. Using this approach, we examined the combined effects of biological and physical transport processes on the changing spatial distribution and reflectance of the bloom. We also estimated net rates of change of PIC concentrations (i.e., the calcium carbonate production via coccoliths) within the bloom. The combined use of satellite, in situ sampling, and HF

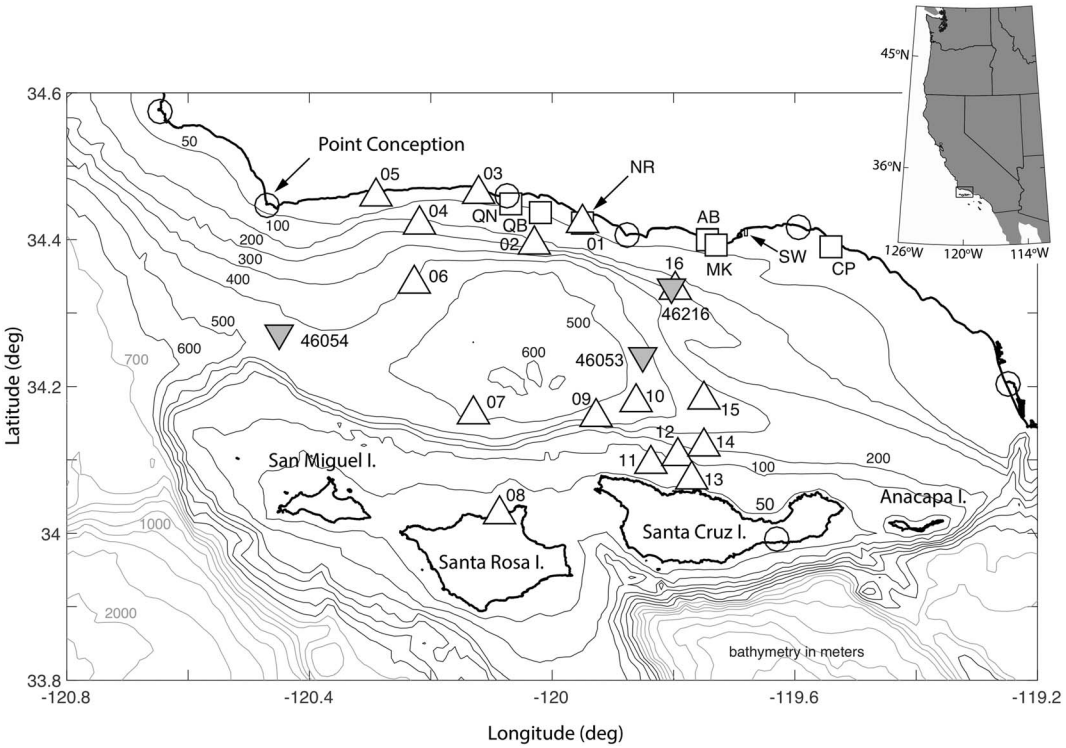

Figure 1. Map of the Santa Barbara Channel indicating locations of samples collected on 5 June (white filled squares; QN, QB, NR, AB, MK, and CP) and 10 June 2015 (white filled triangles; 01 at NR and 02-16). A sample was also collected at NR on 4 June. Open circles along the mainland coast and on Santa Cruz Island show high-frequency radar locations. Inverted gray-filled triangles show NDCB buoys 46053, 46054, and 46216. Small arrow indicates Stearns Wharf (SW). Gray lines are bathymetric contours. Study region shown as rectangle on large-scale, inset map.

radar data can be applied more generally in the coastal ocean to explore the propagation and development of blooms of other phytoplankton groups.

The paper is organized as follows: Section 2 describes the study area in the SBC, data products from remote sensing imagery, in situ sampling, the measurement of surface currents with HF radar, and ancillary data. Section 3 presents the results of the remote sensing analysis including changes in bloom area, changing concentrations of calcified cells and coccoliths in near-surface waters, and patterns of water parcel trajectories inside and outside the bloom. Section 4 discusses the significance of the results, the possible origins of the bloom, and quantitative estimates of changing PIC concentration and their importance, along with use of the method described here in studies of other phytoplankton blooms.

2. Materials and Methods

2.1. Study Location

The bloom of *E. huxleyi* occurred in the SBC in the northern part of the Southern California Bight. The SBC is oriented east-west and is about 100 km long, 40 km wide, with a maximum depth of 600 m in the Santa Barbara basin (Figure 1; Harms & Winant, 1998). It is bounded to the north by the mainland coast and to the south by the Northern Channel Islands. The Santa Ynez Mountains extending eastward from Point Conception block prevailing northwest winds and shelter much of the Southern California Bight. Major currents entering the SBC include the poleward flowing Southern California Counter Current and an equatorward flowing current of upwelled waters from the central California coast, which can interact to form cyclonic eddies within the channel (Harms & Winant, 1998).

2.2. Satellite-Based Remote Sensing to Estimate Bloom Boundaries and Area

The bloom was identified from composite images of remote sensing reflectance (R_{rs}) at 486 and 488 nm measured by the Moderate Resolution Imaging Spectroradiometer on the Aqua satellite and the Visible Infrared

Imaging Radiometer Suite on the Suomi National Polar-orbiting Partnership satellite. These were combined to estimate R_{rs} at 490 nm (turquoise color; hereafter $R_{rs}490$), which corresponds to the peak of spectral reflectance from coccolithophore blooms (Moore et al., 2012). $R_{rs}490$ is well suited for identification of the coccolithophore bloom compared with other remote sensing products, such as chlorophyll a, which would include other noncalcifying phytoplankton groups.

The depth range over which $R_{rs}490$ originates extends from the surface to ~K_d^{-1} where K_d is the attenuation coefficient for downward irradiance. In the clearest natural waters, K_d^{-1} at 490 nm is about 60 m (estimated from Morel et al., 2007). Given the high concentration of cells and detached coccoliths found in the upper 1 m (discussed below and the correlations of Figure 3), we speculate that the depth ranges determining $R_{rs}490$ were significantly reduced from the clear-water value in the SBC during the study period. This is consistent with previous studies that have found cells and coccoliths in coccolithophore blooms to be most abundant near the surface at depths of ≤20 m (reviewed by Zondervan, 2007). However, due to changing cell and coccolith concentrations, the depth ranges determining $R_{rs}490$ were likely variable so there may have been parts of the study area where $R_{rs}490$ was affected by scattering from below the depth range represented by near-surface currents from HF radar measurements.

Figure 2 shows a sequence of $R_{rs}490$ images during 31 May to 18 June 2015 encompassing the study period. Regions obscured by clouds are shown in white and days when $R_{rs}490$ images were entirely obscured by clouds are not included. The spatial distribution of the bloom based on $R_{rs}490$ corresponded well with "true-color" imagery derived from ocean color observations as shown by comparing images on 2 June 2015 in Figure 2c and Figure S1a in the supporting information.

The changing area of the bloom through time was estimated from the sequence of $R_{rs}490$ images of Figure 2. Bloom boundaries were defined as polygons enclosing areas where $R_{rs}490$ exceeded a threshold value $R_{rs}490_{min}$; a value of 0.015 steradian^{-1} (sr^{-1}) for $R_{rs}490_{min}$ was chosen as a good estimator of the boundaries of the bloom. $R_{rs}490_{min}$ is indicated on the color bar of Figure 2. Given that this method focused on changes in bloom area between images, the exact threshold value was not crucial. Changing $R_{rs}490_{min}$ by ±10% around 0.015 sr^{-1} caused about the same percent change in estimates of bloom area (data not shown). To illustrate the procedure for estimating bloom boundaries, Figure S1b shows areas of Figure 2c where $R_{rs}490 \geq 0.015$ sr^{-1} along with the polygon delineating the bloom boundary. In areas where the boundaries of the bloom were covered by clouds, the polygon was subjectively drawn based on the corresponding true-color image such as shown in Figure S1a. The area of the bloom in each image (hereafter bloom area) was defined as the area enclosed by the polygon(s) of the bloom.

2.3. In Situ Sampling and Microscopy

In situ surface water samples (2 L, within the upper 1 m) were collected from stations inside and outside the bloom on 4, 5, and 10 June 2015 (Figure 1). Observers in small vessels used for sample collection identified samples as being inside the bloom by the turquoise color of the seawater. Where remote sensing data corresponding to sampling locations with turquoise-colored seawater were available, they showed elevated values of $R_{rs}490$ (Figures 2e and 2h). Samples were processed for microscopy, flow cytometry, and PIC analyses in the laboratory at the University of California, Santa Barbara, USA.

To confirm the presence of *E. huxleyi*, an aliquot of 50–200 ml from each sample was gently vacuum-filtered through a 13-mm filter membrane of 0.45-μm cellulose nitrate (MF™, EMD-Millipore) or 0.4-μm polycarbonate (Isopore, EMD-Millipore). Filters were dried overnight at room temperature and stored in plastic Petri-slide cases.

Each dried filter was affixed to a 12.7-mm aluminum pin stub using carbon conductive Pelco Tabs™ (Ted Pella, USA) and sputter-coated with gold for 300 s prior to examination under a Zeiss EVO 40 XVP scanning electron microscope at the Santa Barbara Museum of Natural History (CA, USA). Cell concentrations were also determined for samples from 4 and 5 June 2015 using a hemocytometer under light microscopy (200X magnification).

2.4. Flow Cytometry

In situ samples were processed to quantify the percentage of calcified cells (i.e., coccolithophore cells; hereafter % calcified cells) and the ratio of detached-coccoliths to coccolithophores (hereafter detached-

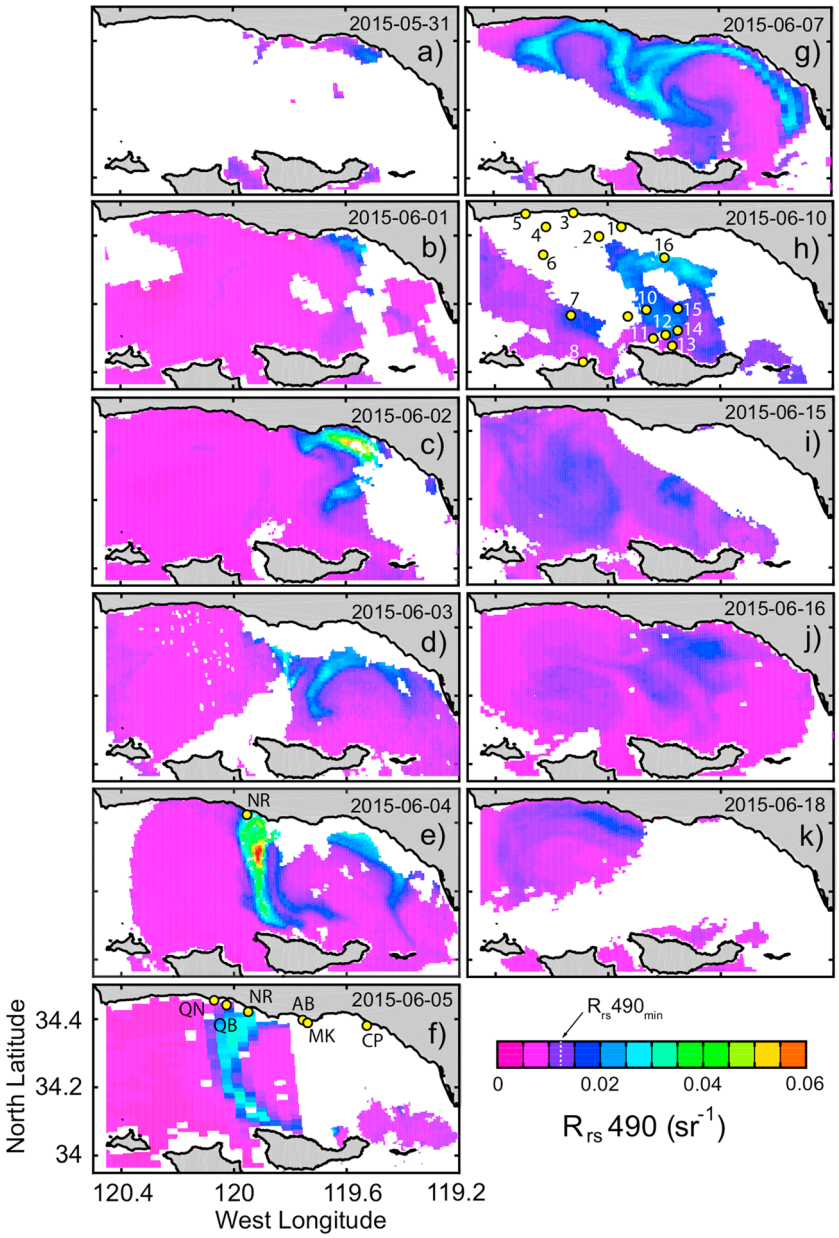

Figure 2. (a–k) Time series of daily composite satellite images showing the changing spatial structure of the coccolithophore bloom visualized by $R_{rs}490$. Yellow circles and labels in panels (e), (f), and (h) indicate in situ sample locations. Color scale is at lower right. White areas indicate no data due to clouds or other factors.

coccoliths:calcified-cell ratio). These metrics provided insights into the state of the bloom at the sampling stations. For example, high detached-coccoliths:calcified-cell ratios indicated an older bloom when cells had reached stationary growth prior to senescence (Balch et al., 1991; Balch et al., 1992; Balch et al., 1993; Holligan et al., 1993). Samples were gently filtered through Nitex mesh (20 μm) in the laboratory to remove large particles exceeding the maximum particle size of the flow cytometer and aliquots of 1–2 ml were drawn from each filtered sample. The percent calcified cells and the detached-coccolith:calcified-cell ratio were determined using a BD Influx Flow Cytometer (BD Biosciences) equipped with three lasers (355, 488, and 640 nm), a small particle detector, and polarization-sensitive detectors. Quality-control beads (Ultra Rainbow Beads; Spherotech) were added as an internal reference immediately before running each sample on the flow cytometer. Samples were first analyzed for approximately 1 min to stabilize the rate at which particles passed through the lasers (i.e., to establish the event rate), after which

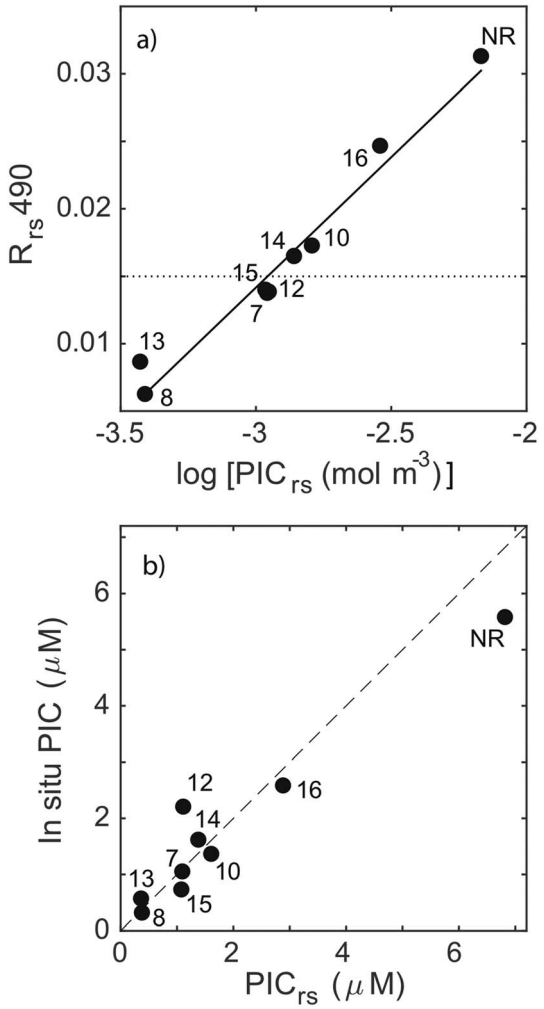

Figure 3. Scatter plot of PIC_{rs} versus (a) $R_{rs}490$ and (b) in situ PIC, for station NR on 4 June and stations 7, 8, 10, and 12–16 on 10 June 2015. Station locations are shown in Figures 1 and 2. Black line in (a) corresponds to the regression: $\log_{10}(y) = 50.05x - 3.71$ ($p = 2.6 \times 10^{-6}$, $R^2 = 0.97$). Horizontal dotted line in panel (a) shows $R_{rs}490_{min} = 0.015$ sr^{-1}. Dashed black line in panel (b) indicates 1:1 relationship. PIC = particulate inorganic carbon.

4,000 events were recorded for each sample. After each sample analysis, the sample intake line was back-flushed to prevent any carry-over from the previous sample. The percent calcified cells and detached-coccoliths:calcified-cell ratio were estimated by categorizing particles into three groups based on size, chlorophyll fluorescence (from a 530- to 540-nm band-pass filter), and polarized forward scatter signal using the cell sorter's software (BD FACS Sortware): (1) noncalcified cells (≥3 μm with chlorophyll and no calcification), (2) calcified cells (≥3 μm, with chlorophyll and calcification), and (3) coccoliths (with calcification and no chlorophyll). The percent calcified cells was calculated as

$$\%\text{calcified cells} = \frac{\text{calcified cells}}{\text{noncalcified cells} + \text{calcified cells}} \times 100 \quad (1)$$

and the detached-coccolith:calcified-cell ratio was calculated as

$$\text{detached}-\text{coccolith : calcified}-\text{cell ratio} = \frac{\text{coccoliths}}{\text{calcified cells}} \quad (2)$$

2.5. PIC

PIC from field samples (hereafter in situ PIC) was measured in the laboratory from aliquots of 33–100 ml that were filtered onto triplicate 25-mm GF/F filters (Whatman, USA) and stored at −20 °C prior to analysis. All filters were placed in sterile 50-ml centrifuge tubes (Falcon, USA). Filters were acidified with a known mass of 0.1-M HNO_3 and placed on a table shaker to agitate at 150 rpm for 24 hr. The acid solution was then passed through a 0.45-μm syringe filter to remove any particulates. Samples were analyzed for Ca^{2+} and Na^+ concentrations using a Perkin-Elmer Optima 7300DV inductively coupled plasma optical emission spectrometer at the Environmental Science Research Laboratory at University of California, Riverside. The concentration of Na^+ was used to correct for excess Ca^{2+} due to residual seawater contamination on the filter.

PIC was also estimated from a satellite remote sensing data product (hereafter PIC_{rs}) described by Balch et al. (2005). PIC_{rs} was significantly correlated with satellite-measured $R_{rs}490$ (Figure 3a) and the value of $R_{rs}490_{min} = 0.015$ sr^{-1} corresponded to $PIC_{rs} = 1.28$ μmol/L based on the regression of Figure 3a. PIC_{rs} was also significantly correlated with in situ PIC based on samples collected on 4 and 10 June 2015 (Pearson correlation: $df = 7$, $p = 2.6 \times 10^{-5}$, $R = 0.96$; Figure 3b) at stations where $R_{rs}490$ observations were available (Figures 2e and 2h).

We assume that PIC mainly comprised calcified cells and coccoliths based on their abundances estimated from flow cytometry. Other sources of PIC such as from resuspended calcified particles due to wave action or river discharge were likely small. The average significant wave height at NDBC buoy 46216 (Figure 1) was small at 0.77 m, and there was no measurable river runoff in the region around the time of the study period. Furthermore, satellite-based observations of suspended particles (based on the particulate backscattering coefficient at 442 nm) in the SBC region were anomalously low during 2015 (Henderikx Freitas et al., 2017).

2.6. Surface Currents and Particle Tracking From HF Radar

Surface currents (upper 1 m) were observed using HF radars along the mainland coast of the SBC and coasts of the Northern Channel Islands (Figure 1). These radars are part of a large regional network maintained by the Southern California Coastal Ocean Observation System (http://sccoos.org). Surface current vectors $\boldsymbol{U}_r$ were computed hourly and interpolated onto a 2-km square grid as described by Emery et al. (2004). In

the interpolation procedure, all radial currents (i.e., from individual radars) within 3 km of each grid point were combined using a least squares procedure to estimate the $\boldsymbol{u}$ (positive eastward) and $\boldsymbol{v}$ (positive northward) components of $\boldsymbol{U}_r$.

Values of $\boldsymbol{U}_r$ were used to simulate Lagrangian particle trajectories over two consecutive tracking periods whose durations corresponded to times between sequential images of $R_{rs}490$ that were mostly cloud free (Figures 2c, 2e, and 2g). The first tracking period was 48 hr (2100 GMT on 2 June to 2100 GMT on 4 June 2015; Figures 2c and 2e), and the second was 72 hr (2100 GMT on 4 June to 2100 GMT on 7 June 2015; Figures 2e and 2g). The times of 2100 GMT were within 31 min or less compared to the image times used to define the tracking periods. Simulated Lagrangian particle trajectories based on HF radar observations were calculated using a fourth-order Runge-Kutta algorithm. Gaps in coverage of a few hours were filled using empirical orthogonal functions. The particle tracking procedure is described in more detail by Emery et al. (2006).

During each tracking period, 59,860 simulated particles (hereafter drifters) were started at random locations within the 5,175-km^2 study domain encompassing the SBC. Drifter starting locations were grouped into three categories: inside the bloom area, outside the bloom area, or under clouds. Drifter ending locations were grouped into six categories: (1) inside bloom area but not ashore, (2) ashore inside bloom area, (3) outside bloom area but not ashore, (4) ashore outside bloom area, (5) under clouds, or (6) out of the study region. Drifters were considered ashore and their trajectories ended when they encountered boundaries of bloom polygons adjacent to the shore. Drifters that started or ended under clouds were not used to classify trajectories in the analysis.

We applied the method described by Ullman et al. (2006) and Ohlmann et al. (2012) to account for trajectory errors. The method estimates surface current velocity $\boldsymbol{U}$ averaged over the 1-hr trajectory segments as

$$\boldsymbol{U}=\boldsymbol{U}_r+\boldsymbol{u}' \tag{3}$$

where $\boldsymbol{u}'$ is the velocity uncertainty due to unresolved subgrid-scale motions (e.g., turbulence and submesoscale advection) and radar measurement errors.

Hourly estimates of $\boldsymbol{u}'$ were randomly drawn (with replacement) from probability density distributions of the u' and v' components of $\boldsymbol{u}'$ previously measured in the SBC as described by Ohlmann et al., (2012). In that study $\boldsymbol{u}'$ was estimated as $\boldsymbol{U}-\boldsymbol{U}_r$ where $\boldsymbol{U}$ was assumed to equal the drifter velocity and $\boldsymbol{U}_r$ was interpolated hourly to locations where $\boldsymbol{U}$ was measured. Drifter tracks used by Ohlmann et al. (2012) to estimate u' and v' were obtained from the same general area of the SBC where the coccolithophore bloom occurred. The tracks were also obtained during most months of the year, including spring, and therefore should provide reasonable estimates of $\boldsymbol{u}'$ for uncertainty calculations to follow.

To apply the error method, 100 trajectories assuming $\boldsymbol{U}=\boldsymbol{U}_r$ in 3 were randomly chosen from both tracking periods using three combinations of starting and ending locations: (a) drifters starting and ending inside the bloom (i.e., within the polygons delineating the bloom), (b) drifters starting inside and ending outside the bloom, and (c) drifters starting outside and ending inside the bloom. For example, $\boldsymbol{u}'$ was added to $\boldsymbol{U}_r$ at each 1-hr time step according to 3 for each of the 100 trajectories in combination (a). Then the ending trajectory locations were classified as being inside the bloom, outside the bloom, or under clouds. This was repeated 100 times for each of the 100 trajectories in combination (a) to produce 10^4 total trajectories. Any trajectories ending outside the bloom or under clouds did so only due to contributions from nonzero $\boldsymbol{u}'$. Therefore, we interpreted the fraction of trajectories ending outside the bloom as a quantitative measure of the effects velocity uncertainty or radar errors (i.e., nonzero $\boldsymbol{u}'$). The procedure was similarly applied to the other combinations such that any trajectories ending inside the bloom (or under clouds) for combination (b) or ending outside the bloom for combination (c) did so only due to the effects of nonzero $\boldsymbol{u}'$. Figure S2 shows the starting locations (Figures S2a–S2c) and ending locations (Figures S2d–S2f) resulting from this procedure for the three combinations (a), (b), and (c) respectively, during the 48-hr tracking period.

2.7. Ancillary Data

Additional publically available data sets were used to describe the environmental conditions existing within the SBC before and during the bloom. Monthly observations of temperature profiles and nutrients at coastal

sites in the SBC were downloaded from the Santa Barbara Coastal Long Term Ecological Research project (SBC LTER) website (http://sbc.lternet.edu/data/) as were time series of temperature near the surface, at middepth, and near the bottom seafloor at moorings in 10- to 15-m water depths along the mainland coast. Biweekly observations of harmful algal bloom taxa present at Stearns Wharf were downloaded from the Southern California Coastal Ocean Observation System website (http://sccoos.org/data/habs/).

3. Results

3.1. Satellite Time Series of Bloom Development

The bloom was first detected offshore of the mainland coast on 31 May 2015 from a satellite image that was mostly covered by clouds (Figure 2a). A relatively intense bloom signal based on $R_{rs}490 > R_{rs}490_{min}$ persisted until 10 June (Figure 2h). The correlation among $R_{rs}490$, PIC_{rs}, and in situ PIC (Figure 3) indicates that PIC concentrations exceeded 1.28 μmol/L until 10 June. After 10 June clouds covered the study area until 15 June when a weakened bloom signal continued in the SBC until 18 June (Figure 2k).

On 2 June, the bloom area covered 366 km^2 (Figures 2c and S1b). By 4 June 2015, the bloom area had expanded to 769 km^2 and developed a southward extension across the SBC (Figure 2e); the maximum $R_{rs}490$ of 0.064 sr^{-1} on 4 June was the highest value observed during the bloom. During 4–5 June most of the southward extension moved westward while its southernmost part curved eastward along the northern coast of Santa Cruz Island. By 7 June, the maximum $R_{rs}490$ decreased to 0.032 sr^{-1}, while the bloom area had further expanded to 1,220 km^2 and spread over most of the length of the SBC along the mainland coast (Figure 2g).

On 10 June bloom values of $R_{rs}490$ continued to exceed $R_{rs}490_{min}$ with a maximum of 0.027 sr^{-1}, although coverage was sparse due to clouds (Figure 2h). During subsequent days when parts of the bloom were visible on 15, 16, and 18 June, images showed reduced $R_{rs}490$, near $R_{rs}490_{min}$, with maximum values of 0.016, 0.016, and 0.015 sr^{-1}, respectively (Figures 2i–2k).

3.2. In Situ Observations of Bloom Development

Scanning electron microscopy imagery confirmed the presence of *E. huxleyi* in samples collected within the bloom at Naples Reef (NR, Figure 1) on 4 and 5 June with maximum calcified-cell concentrations of 5.7×10^6 and 2.55×10^6 cells per liter, respectively. This concentration range is almost an order of magnitude greater than the previously reported maximum concentration of 6.2×10^5 cells per liter in the Southern California Bight (Winter, 1985), both above the *E. huxleyi* bloom thresholds suggested by Tyrrell and Merico (2004). Additional samples collected within the bloom at Arroyo Quemado (QB), Arroyo Burro (AB), Mohawk Reef (MK), and Carpinteria (CP) on 5 June also contained *E. huxleyi* (Figure 1). On 5 June, calcified-cell concentrations were highest at NR and decreased to the west at QB (3.16×10^5 cells per liter) and to the east at AB, MK, and CP (1.13×10^6, 9.33×10^5, and 3.00×10^5 cells per liter, respectively).

Changes during 4–10 June in percent calcified-cells, detached-coccolith:calcified-cell ratio, and in situ PIC were consistent with an *E. huxleyi* bloom that transitioned from a growing state to a senesced or decaying state. Figure 4 partitions sampling stations into quadrants (one is unoccupied) based on % calcified-cells and detached-coccolith:calcified-cell ratio. On 4 and 5 June all but two stations (stations QN and CP) fell in the upper left quadrant where percent calcified-cells >25% coincided with values of detached-coccolith:calcified-cell ratio < 40. This indicated high percentages of coccolithophores with low numbers of detached coccoliths per coccolithophore cell, a characteristic of a growing bloom (Balch et al., 1991; Balch et al., 1992; Balch et al., 1993; Holligan et al., 1993). By 10 June the situation had reversed when all stations had % calcified-cells <25% and most fell into the lower right quadrant with detached-coccolith:calcified-cell ratios >40, which was consistent with a decaying or senesced bloom. All but one station (station 7) in the upper left and lower right quadrants had in situ PIC ≥ 1.28 μmol/L, which corresponded to $R_{rs}490 \geq R_{rs}490_{min}$ and indicated stations within the bloom. Points in the lower left quadrant corresponded to low percentcalcified-cells and low detached-coccolith:calcified-cell ratios. Only one of these stations had in situ PIC > 1.28 μmol/L (station 14). We speculate that the stations in the lower left quadrant were located in areas where other types of phytoplankton were present in high concentrations and where coccolithophore and coccolith concentrations were below bloom levels, which appears to be typical within the SBC.

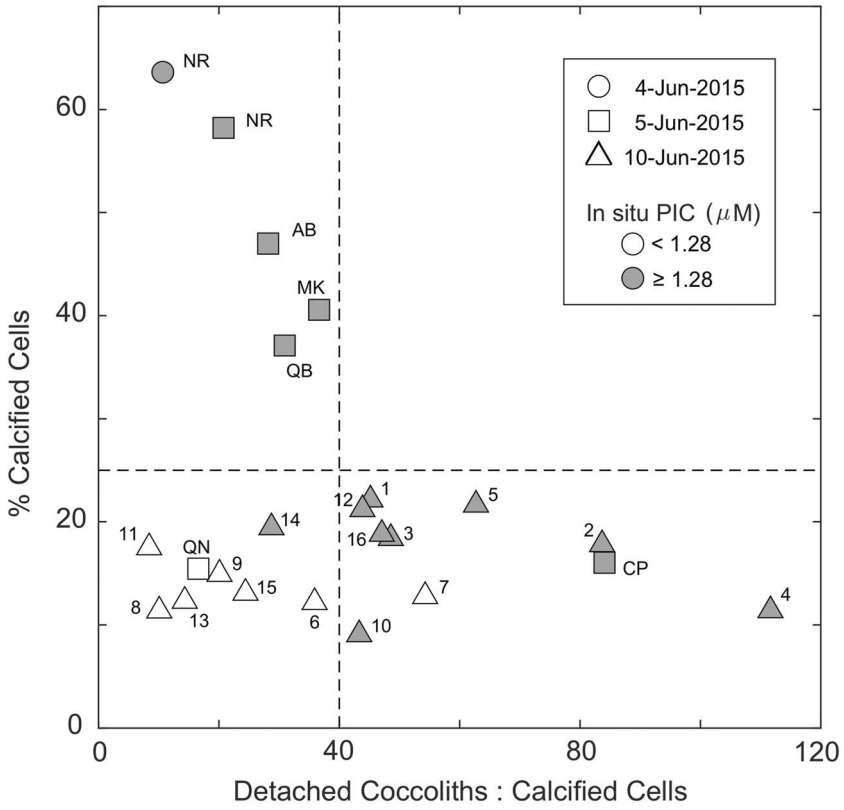

Figure 4. Scatter plot of % calcified cells versus detached-coccoliths:calcified-cell ratio for samples collected on 4, 5, and 10 June 2015. Symbols indicate collection dates of samples. Gray-filled symbols indicate in situ PIC ≥ 1.28 μM; this value corresponds to $R_{rs}490 \geq R_{rs}490_{min} = 0.015\ sr^{-1}$ obtained from the regression line in Figure 4a. Labels identify stations shown in Figures 1 and 2. Vertical dashed line indicates detached-coccoliths:calcified-cell ratio = 40; horizontal dashed line indicates % calcified cells = 25%. PIC = particulate inorganic carbon.

3.3. Bloom Development and Surface Currents

Water parcel trajectories were used to examine the changing spatial structure of the bloom during the two tracking periods (48 hr, 2–4 June; 72 hr, 4–7 June). Of the 59,860 drifters simulated in each period, most remained within the study area: 93% during the 48-hr tracking period and 91% during the 72-hr period. For the 48- and 72-hr tracking periods, 42,329 drifters (71%) and 43,654 drifters (73%), respectively, started in cloud-free regions of the study area (Table S1). About 2% of these drifters ended under clouds after the 48-hr tracking period and 42% ended under clouds after the 72-hr tracking period. For examining the changing structure of the bloom, only trajectories that started and ended in cloud-free regions were used. Results from these trajectories are summarized below and are listed under columns in Table S1 with headings $\%^{nc}$.

3.3.1. Trajectories of Advected Bloom Parcels

Most drifters starting in the bloom remained in the bloom during the tracking periods; these comprised 78% of drifters not ending under clouds from the 48-hr tracking period and 53% from the 72-hr tracking period. These results indicated that advection by surface currents during the 48-hr tracking period contributed to the westward extension of the bloom along the mainland coast (i.e., red points, east of a to a′ in Figures 5a and 5b). Results also indicated that advection contributed to the southwestward expansion of the central part of the bloom during the 72-hr tracking period (i.e., red points, g to g′ in Figures 6a and 6b). Subsets of trajectories illustrate the different pathways followed by the drifters in the bloom during the tracking periods (Figures 5b and 6b).

After recalculating trajectories incorporating nonzero $\boldsymbol{u}'$ (velocity uncertainty and radar errors) according to 3, about 80% and 84% of drifters from the 48- and 72-hr tracking periods, respectively, still ended in the bloom (Table S2). For the 48-hr tracking period, 15% ended outside the bloom and 4% ended under clouds; for the 72-hr tracking period these fractions were 11% and 5%, respectively. Together these indicate an upper

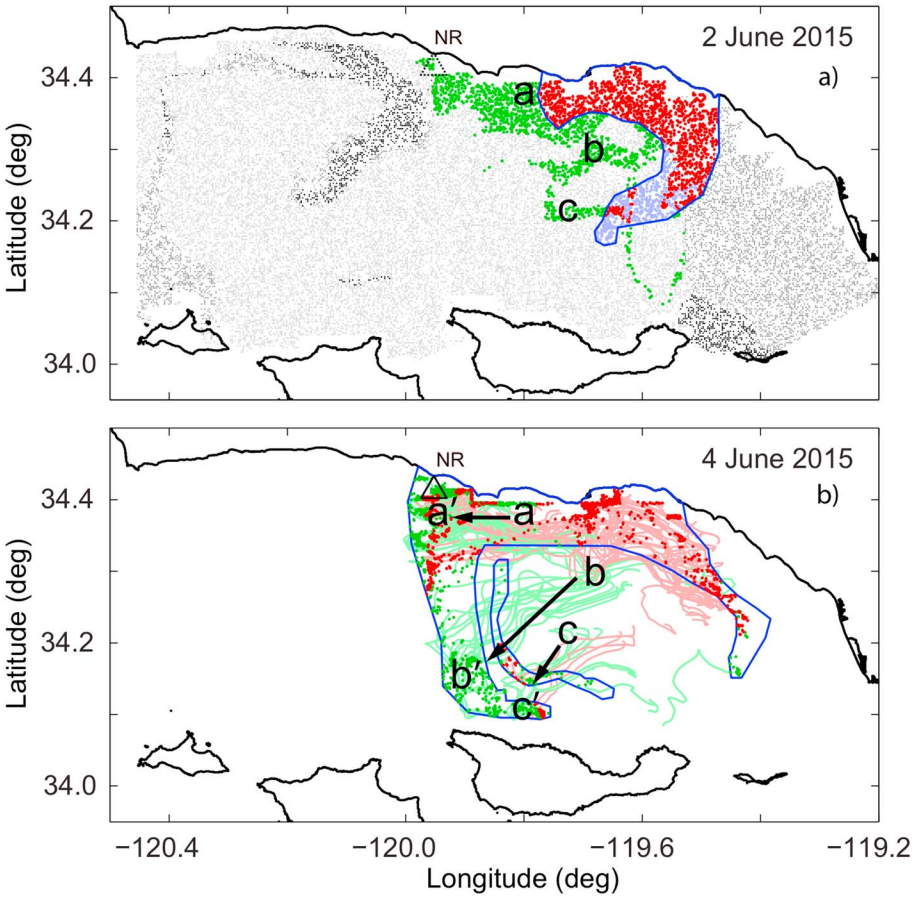

Figure 5. (a) Drifter simulations based on hourly high-frequency radar data. Dots show beginning locations of drifters for the 48-hr tracking period (2–4 June 2015). Dot color indicates drifter movement: drifters started and ended inside the bloom (red); drifters started inside the bloom and ended outside the bloom (lavender); drifters started outside the bloom and ended inside the bloom (green); drifters started outside the bloom and ended outside the bloom (light gray); drifters started or ended under clouds (dark gray); drifters ended outside the study area (black). (b) Hindcast trajectories (lines) and ending locations (dots) are shown for a subset of drifters ending in the bloom. Colors indicate drifter locations starting inside the bloom (red) or outside the bloom (green). The bloom boundary each day is indicated by the blue polygons. Labels of a, b, and c are in the same locations in panels (a) and (b). Black triangle in panel (b) indicates location of sample collected at NR on 4 June. Dotted triangle indicates this location on 2 June.

bound of ~20% uncertainty in the ending locations with respect to the bloom due to the influences of unresolved motions and measurement error. This is an upper bound because some drifters ending under clouds may also have ended in the bloom.

3.3.2. Trajectories of Senescing Bloom Parcels

Other trajectories exhibited $R_{rs}490$ values that started above and ended below bloom levels (lavender dots, Figures 5a and 6a). These comprised 22% of drifters during the 48-hr tracking period and 40% of drifters during the 72-hr tracking period (Table S1). They exceeded the percentages of trajectories that started below and ended above bloom levels by factors of 2.74 and 2.50 for the 48- and 72-hr tracking periods, respectively. The greater fraction of senescing bloom trajectories than growing bloom trajectories is consistent with an overall decline in peak values of $R_{rs}490$ after 4 June (Figure 2). Here we use the term senescing to identify trajectories where $R_{rs}490$ levels fall below $R_{rs}490_{min}$ but recognize that other nonconservative processes, such as unresolved physical transport processes, may also reduce $R_{rs}490$ levels. Most trajectories interpreted as senescing bloom parcels originated at the southern tip of the bloom during the 48-hr tracking period (east of c and southeast of b, Figure 5a). During the 72-hr tracking period they originated in two locations near the mainland coast (east of d and southeast of g, Figure 6a) and in the southern half of the southward extension, including a detached segment of the bloom (southwest of e, Figure 6a).

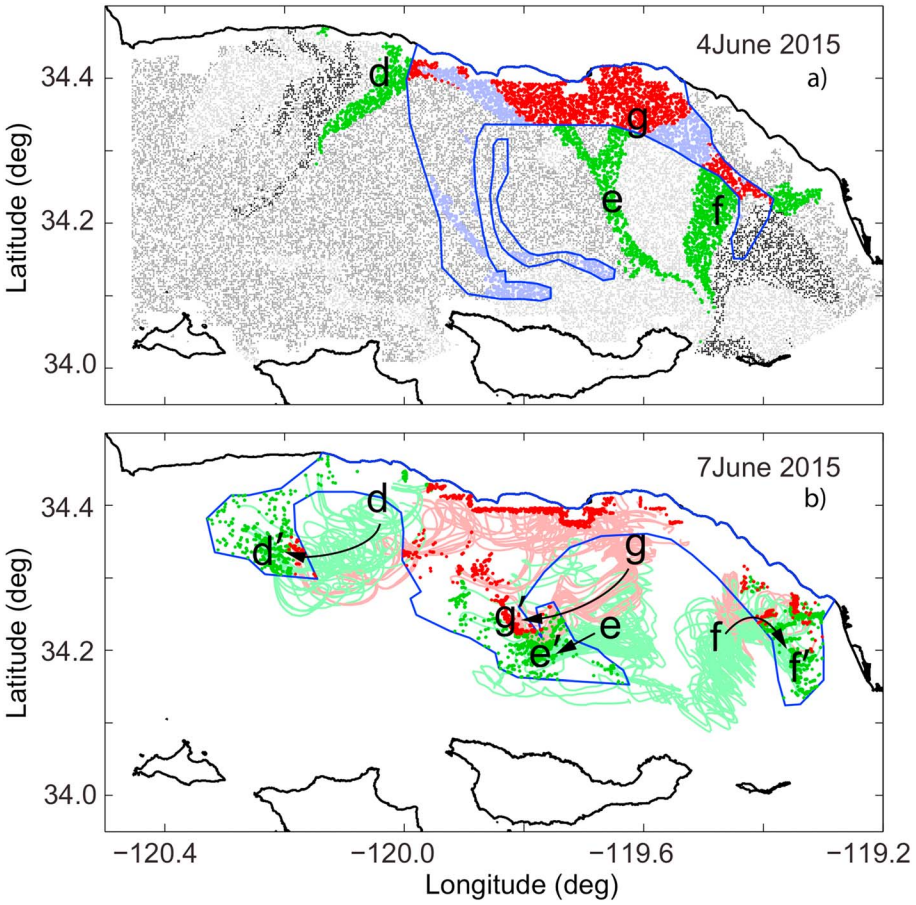

Figure 6. As in Figure 5 but for the 72-hr tracking period (4–7 June 2015). Labels of d, e, f, and g are in the same locations in panels (a) and (b).

After recalculating trajectories to examine the effects of velocity uncertainty (nonzero $\boldsymbol{u}'$), 70% of drifters that started inside the bloom and ended outside the bloom with $\boldsymbol{u}' = 0$ during the 48-hr tracking period still did so (Table S2). Of the remaining 30%, 28% ended inside the bloom and 2% ended under clouds. For the 72-hr tracking period these fractions were 74%, 15%, and 11%, respectively (Table S2).

3.3.3. Trajectories of Growing Bloom Parcels

Trajectories over which $R_{rs}490$ levels increased to bloom levels were indicated by the fraction of drifters that started outside the bloom and ended inside the bloom (green dots, Figures 5a and 6a). For the 48-hr tracking period these comprised 8% of drifters not ending under clouds and for the 72-hr tracking period they comprised 16% of drifters not ending under clouds (Table S1). For the 48-hr tracking period, 64% of drifters that started outside the bloom and ended inside the bloom with $\boldsymbol{u}' = 0$ still did so after accounting for velocity uncertainty (nonzero $\boldsymbol{u}'$; Table S2). Of the remaining 36%, 35% ended outside the bloom and 1% ended under clouds. For the 72-hr tracking period, 60% still ended in the bloom, 26% ended outside the bloom, and 14% ended under clouds.

Drifters starting west of the bloom on 2 June near the mainland coast were subsequently incorporated into the bloom by 4 June (a to a′, Figure 5b). In situ sampling at NR on 4 June corroborated this result. On 2 June the location of NR (dotted triangle, Figure 5a) was outside the bloom based on the bloom boundary shown in Figure 5a (no in situ samples at NR were available on 2 June). On 4 June in situ sampling at NR confirmed the presence of *E. huxleyi* and values of in situ PIC exceeded 1.28 μmol/L (corresponding to a $R_{rs}490$ value of 0.015 sr^{-1}), supporting the interpretation of a growing bloom population (Figure 4). Farther offshore, many drifters that started outside the bloom ended inside near the tip of an extension of the bloom across the central SBC (green points, b to b′ and c to c′, Figure 5b).

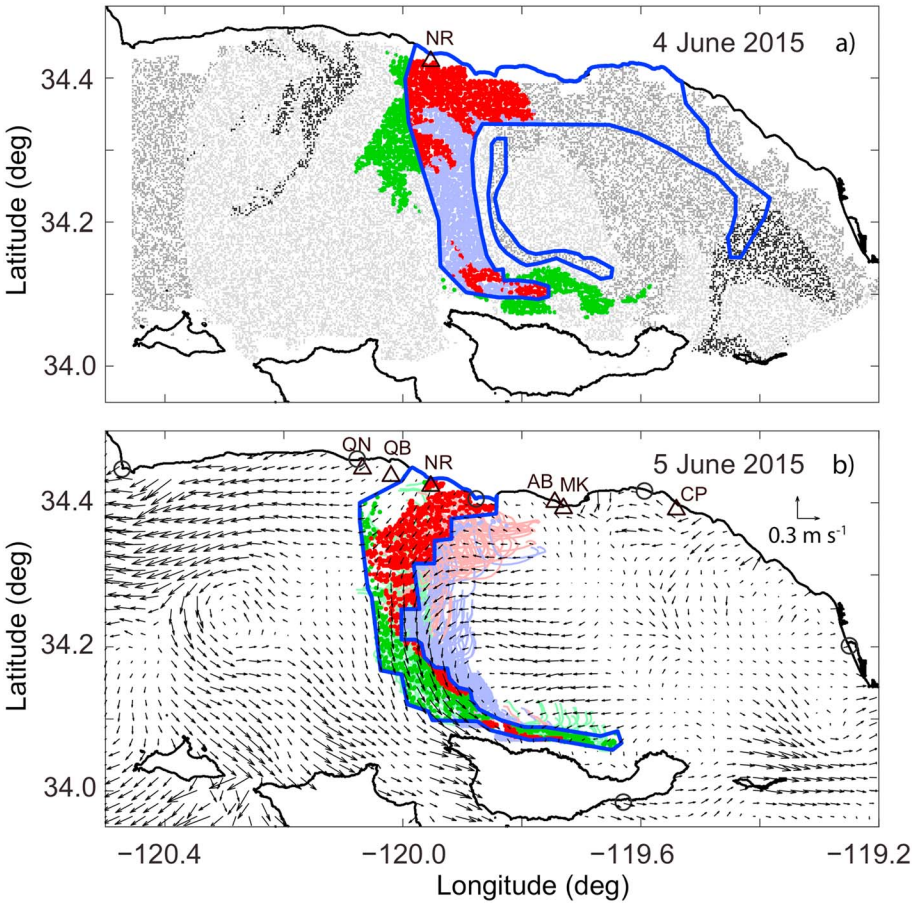

Figure 7. As in Figure 5 but during 4–5 June 2015. Arrows in panel (b) show surface current vectors averaged during 2100 GMT on 4 June to 2100 GMT on 5 June 2015. These span the times between images used to estimate the bloom boundaries (blue polygons). Lavender lines in panel (b) show hindcast trajectories of drifters that started inside the bloom and ended outside the bloom. Open circles are high-frequency radar sites. Triangles show sampling locations on 4 and 5 June 2015. Scale for surface current vectors is in the upper right of panel (b).

Trajectories with $R_{rs}490$ increasing from below to above bloom levels during the 72-hr tracking period (4–7 June) formed two extensions of the bloom along the mainland coast, one westward and the other eastward (green points, d to d′ and f to f′, respectively, Figure 6b). Advection to the southwest combined with growth also changed the central extension of the bloom (red points, g to g′ and green points, e to e′, Figure 6b). The evolution of the extension was further explored by evaluating changes between 4 and 5 June (Figures 7a and 7b). Growth along the western side of the extension (green dots, Figure 7) combined with southward advection moved the western bloom boundary farther west. At the same time senescence or losses due to unresolved physical processes in the eastern side (lavender dots) contributed further to westward movement of the extension over the 24-hr period. Surface currents spanning the senescing and growing parts of the extension were mainly southward with a westward component in the northern part of the extension and an eastward component in the southern part. Eastward currents along Santa Cruz Island combined with growth to move the southern tip region of the extension eastward.

In situ sampling corroborated the nearshore position of the bloom boundary where data were available (section 3.2). In situ sampling confirmed that the main component of the coccolithophore bloom was *E. huxleyi* at NR on 4 and 5 June, consistent with NR being in the bloom on those dates (red dots at NR, Figures 7a and 7b). *E. huxleyi* were also found at QB, but not 4.5 km to the west at QN (Figure 7b), suggesting that the boundary was between these stations. However, Figure 7b indicates that QB was just west of the boundary, although uncertainty in the boundary location may have resulted from the highly inclined

viewing angle from the 5 June satellite pass. Symbols in Figure 2f show QB at the western edge of the region of elevated $R_{rs}490$ and QN farther away from the edge to the west. In situ sampling at AB, MK, and CP all found *E. huxleyi,* but no $R_{rs}490$ data were available at those sites on 5 June (Figures 7b and 2f).

4. Discussion and Summary

4.1. Conditions Selecting for the Bloom

Ocean conditions in the SBC preceding the bloom of *E. huxleyi* included low nutrient concentrations, stratified waters, and the prior occurrence of a diatom bloom. These conditions are in agreement with previous studies by Iglesias-Rodriguez et al. (2002) using global analysis of coccolithophore bloom populations (largely represented by *E. huxleyi*). Additionally, due to the warm anomaly of 2013–2015 and the following El Niño in 2015 (Bond et al., 2015; Di Lorenzo & Mantua, 2016) waters in the SBC were unusually warm during all of 2015 with monthly temperature anomalies up to +4.6 °C (7- to 10-m depths, Reed et al., 2016). Increased temperatures have been linked to expansions of *E. huxleyi* into the Arctic (Neukermans et al., 2018) and increased abundances across the North Atlantic (Rivero-Calle et al., 2015). Modeling studies by Krumhardt et al. (2017) support some of these observations, suggesting that increases in sea surface temperature (~2–3 °C) lead to faster coccolithophore growth rates globally (>10% increase), though decreased nutrient availability (from warming-induced increases in stratification) enhances calcification at the cost of growth (~25% decrease), which might be in disagreement with our observations.

Monthly nitrate anomalies measured along the mainland coast of the SBC by the SBC LTER were negative for all months in 2014 and 2015 (Reed et al., 2016), which could have selected for the coccolithophore bloom (Iglesias-Rodriguez et al., 2002). Increased stratification was indicated by positive monthly anomalies in vertical temperature differences ($T_{surface} - T_{bottom}$; water depths 15 m or less) throughout 2015 at the SBC LTER moorings along the mainland coast (data not shown).

The SBC phytoplankton bloom population composition in 2015 followed the typical successional dynamics of diatoms followed by coccolithophores (Sieracki et al., 1993; Smayda, 1989). Sampling of phytoplankton at Stearns Wharf (SW, Figure 1) on 11 May 2015 measured concentrations of both large and small forms of pennate diatoms within the genus *Pseudo-nitzschia* that each exceeded 1.1×10^5 cells per liter. Concentrations from 14 April to 15 June 2015 (excluding 11 May) ranged from 0 to 2.3×10^4 cells per liter so the bloom concentrations were significantly larger than prevailing nonbloom concentrations before and after the bloom. Blooms of coccolithophores generally occur following the decline of large diatom blooms (Holligan et al., 1993), such as the one observed at SW. The postdiatom bloom environment can be rapidly exploited by *E. huxleyi*, which possesses a high affinity for inorganic nutrients (Eppley et al., 1969; Riegman et al., 2000) and the ability to utilize organic forms of N and P (Benner & Passow, 2010).

We speculate that the environmental conditions in the SBC governed the onset and development of the *E. huxleyi* bloom, namely, a highly stratified water column with anomalously high temperatures that was poor in inorganic nitrate and potentially high in organic forms of nitrogen due to the declining diatom bloom (Tyrrell & Merico, 2004). A similar coastal bloom of *E. huxleyi* occurred one month later ~300 km north in Monterey Bay, CA, USA, during July 2015 (unpublished data) suggesting that similar conditions may have been present elsewhere in the California Current during this time period.

4.2. Assessing Coccolithophore Bloom Development

We assume that coccolithophores are advected in near-surface Lagrangian water parcels while local-scale, nonconservative biological and physical processes change coccolithophore and coccolith concentrations within the water parcels. These concentration changes are reflected in the variable patterns of $R_{rs}490$ (Figure 2) and as gain and loss of drifters from the bloom area (Figures 5–7) as $R_{rs}490$ levels rise above or fall below the threshold value $R_{rs}490_{min}$. Many nonconservative biological processes, such as growth, grazing, and viral lysis, can cause these changes as a coccolithophore bloom ages (e.g., Bratbak et al., 1993; Evans et al., 2007). Nonconservative physical processes capable of causing similar changes in concentrations and $R_{rs}490$ include gravitational sinking of coccolithophores and coccoliths, vertical mixing, and horizontal dispersion (Balch et al., 2009). Submesoscale flows at density fronts can lead to localized upwelling and

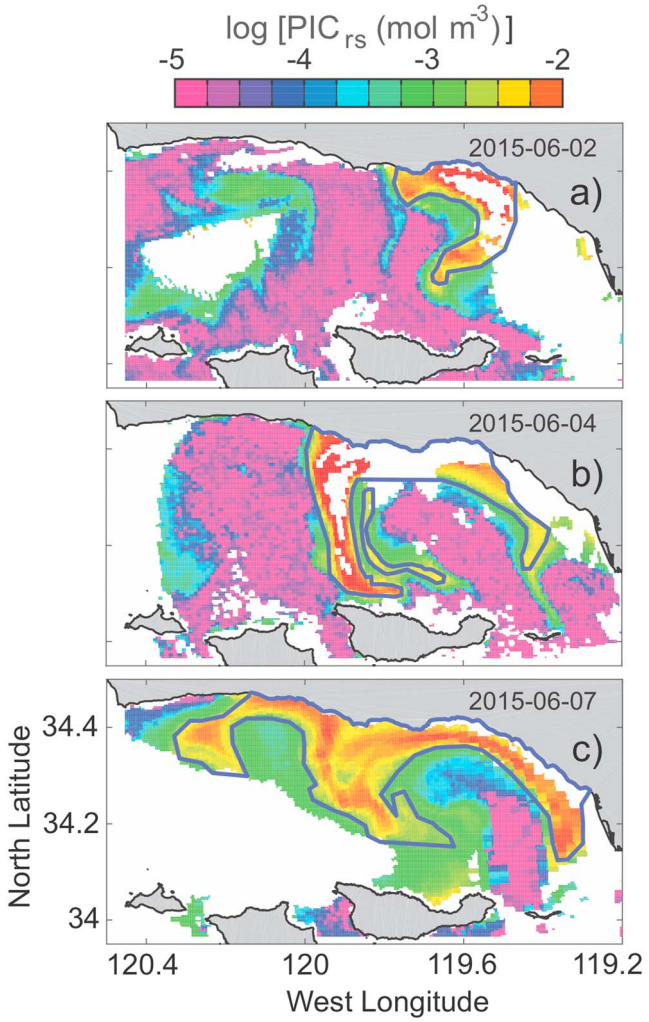

Figure 8. Satellite images of particulate inorganic carbon (PIC_{rs}) distributions on (a) 2, (b) 4, and (c) 7 June 2015. Color bar at top shows log PIC_{rs}. White areas indicate where PIC_{rs} data were not available, due to cloud cover or other factors. Blue polygons indicate bloom boundaries based on $R_{rs}490_{min}$ as described in the text.

downwelling on horizontal scales on the order of a few kilometers and smaller, which may also lead to enhanced rates of particle aggregation and removal (e.g., Capet et al., 2008; Estapa et al., 2015).

Drifter trajectories starting and ending in the bloom are consistent with populations of coccolithophores and coccoliths whose concentrations persist at bloom levels throughout the tracking periods. The changing spatial patterns of these drifters are likely driven primarily by advection and they comprise the most common bloom-associated trajectories during both tracking periods (Figures 5b and 6b). These results support the importance of advection in driving the spatial propagation of the bloom through time. However, Figure 7 suggests that during 4–5 June westward movement of the bloom resulted in part from growth on one side and senescence on the opposite side of the bloom.

During both tracking periods more trajectories exited the bloom than entered the bloom as quantified by the ratio of the corresponding percentages as discussed in section 3.3.3. However, the magnitude of change (defined as the ratio between 72- and 48-hr periods) in trajectories leaving the bloom (1.82) was greater than the magnitude in change of the bloom area (1.59) between the two periods. This is consistent with the overall, but not monotonic, decline in $R_{rs}490$ within the bloom during 2–7 June (Figure 2). Variability in $R_{rs}490$ can result from coccolithophore cell growth and loss, shedding of coccoliths, or both, which complicates the interpretation of the overall decrease in $R_{rs}490$.

4.3. Quantifying Calcification Rates

Quantifying rates of change of PIC concentrations is important for constraining the $CaCO_3$ budget and, more generally, for understanding the carbonate system in the upper ocean (e.g., Iglesias-Rodriguez et al., 2002). The determination of calcification rates from field observations of PIC concentrations is complicated by the advection of water parcels confounding the estimation of changes in PIC. Here we estimate the changes of PIC following surface water parcels, D (PIC)/Dt, based on the images of PIC_{rs} (Figure 8) on 2, 4, and 7 June 2015 and water parcel trajectories computed from the HF radar-derived surface currents. These estimates are net rates in which growth increases are offset by losses due to biological processes and physical processes (e.g., mixing, and particle sinking to depth). The trajectories provided an objective basis for connecting between images the starting and ending locations and corresponding PIC_{rs} values. This allowed estimation of net changes in PIC_{rs} concentrations (ΔPIC_{rs}) along trajectories over the time interval between images Δt. D (PIC_{rs})/Dt was estimated as

$$\frac{D(PIC_{rs})}{Dt} \approx \frac{\Delta PIC_{rs}}{\Delta t} = \frac{[PIC_{rs}(t_2) - PIC_{rs}(t_1)]}{t_2 - t_1} \quad (4)$$

where $PIC_{rs}(t_1)$ and $PIC_{rs}(t_2)$ were interpolated to the starting and ending locations of the trajectories at times of the satellite images t_1 and t_2, respectively, that defined each tracking period. Histograms were then computed to examine how the distributions of D (PIC_{rs})/Dt changed between the tracking periods.

To account for uncertainty in the ending locations of trajectories due to nonzero $\boldsymbol{u}'$ in 3, D (PIC_{rs})/Dt was also estimated with from PIC_{rs} interpolated to the ending locations of the trajectories with nonzero $\boldsymbol{u}'$ as described in section 2.6. In doing so, we assumed the largest errors in estimating D (PIC_{rs})/Dt resulted from errors in estimating $PIC_{rs}(t_2)$ in 4 due to uncertainty in ending locations of trajectories. Figure S3 shows three examples of ending locations of trajectories computed with $\boldsymbol{u}' = 0$ (white circles) and 100 scattered ending

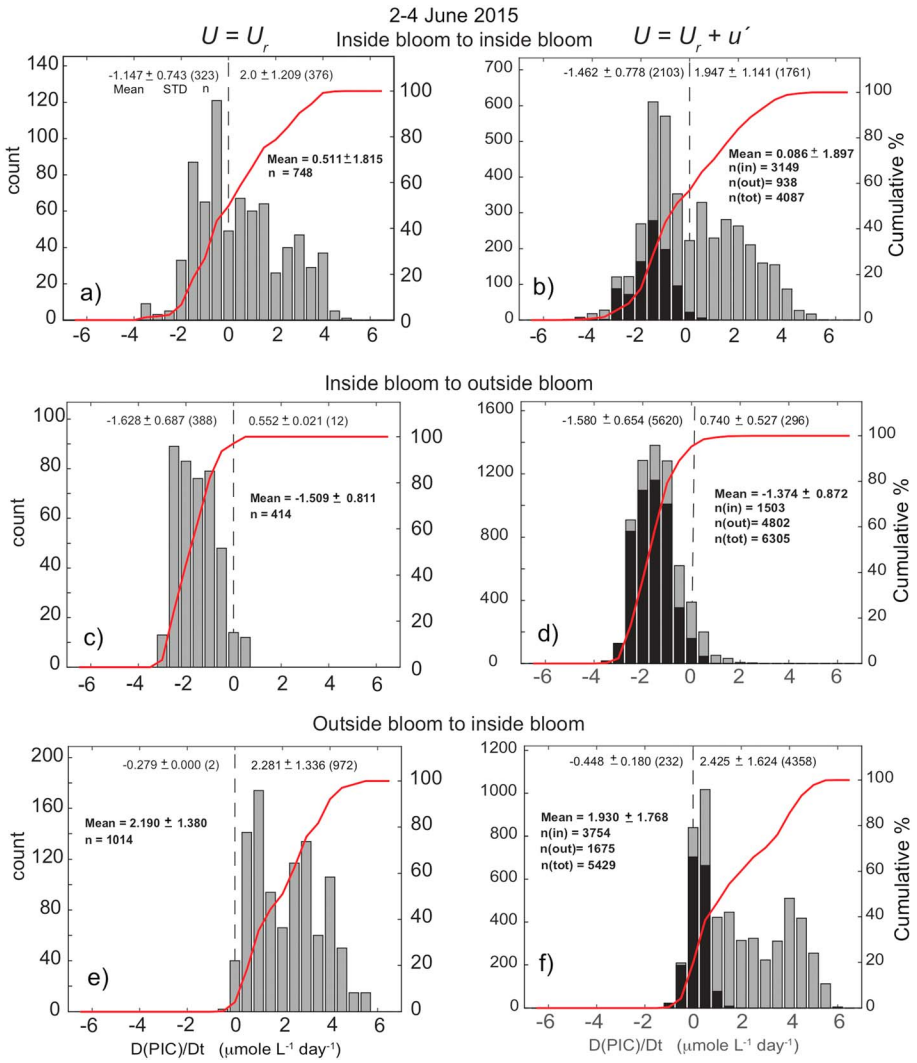

Figure 9. Histograms (stacked gray and black bars) and cumulative distributions (red lines) of D (PIC_{rs})/Dt as defined in 4 for the 48-hr tracking period (2–4 June 2015). Histograms for trajectories starting and ending inside the bloom using (a) $\boldsymbol{U = U_r}$ or (b) $\boldsymbol{U = U_r + u'}$ in 3. Histograms for trajectories starting inside and ending outside the bloom using (c) $\boldsymbol{U = U_r}$ or (d) $\boldsymbol{U = U_r + u'}$. Histograms for trajectories starting outside and ending inside the bloom using (e) $\boldsymbol{U = U_r}$ or (f) $\boldsymbol{U = U_r + u'}$. Black segments of histogram bars indicate trajectories that ended outside the bloom. Bold text indicates overall means, standard deviations and total numbers inside and outside the bloom of D (PIC_{rs})/Dt values. Means, standard deviations, and numbers of positive (negative) D (PIC_{rs})/Dt values are shown in upper right (left) of each panel.

locations computed with nonzero $\boldsymbol{u'}$ (black dots). The underlying satellite image shows that the scattered ending locations span a range of $PIC_{rs}(t_2)$ values, which lead to errors in D (PIC_{rs})/Dt.

Histograms revealed clear differences in D (PIC_{rs})/Dt distributions over the two tracking periods (Figures 9 and 10). For example, during the first tracking period D (PIC_{rs})/Dt values for trajectories starting and ending in the bloom with $\boldsymbol{U = U_r}$ ranged from −4 to +5 μmol·L^{-1}·day^{-1} (Figure 9a) compared with ±2 μmol·L^{-1}·day^{-1} during the second tracking period (Figure 10a). Overall, means of D (PIC_{rs})/Dt were low during both tracking periods (bold text, Figures 9a, 9b, 10a, and 10b) such that positive and negative distributions D (PIC_{rs})/Dt were nearly compensating. Velocity uncertainty in trajectories computed with $\boldsymbol{U = U_r + u'}$ resulted in some trajectories ending outside the bloom during both periods (black segments, Figures 9b and 10b) although, the widths of the distributions of D (PIC_{rs})/Dt (e.g., standard deviations) were robust with respect to velocity uncertainty. Narrowing of the D (PIC_{rs})/Dt distributions between the

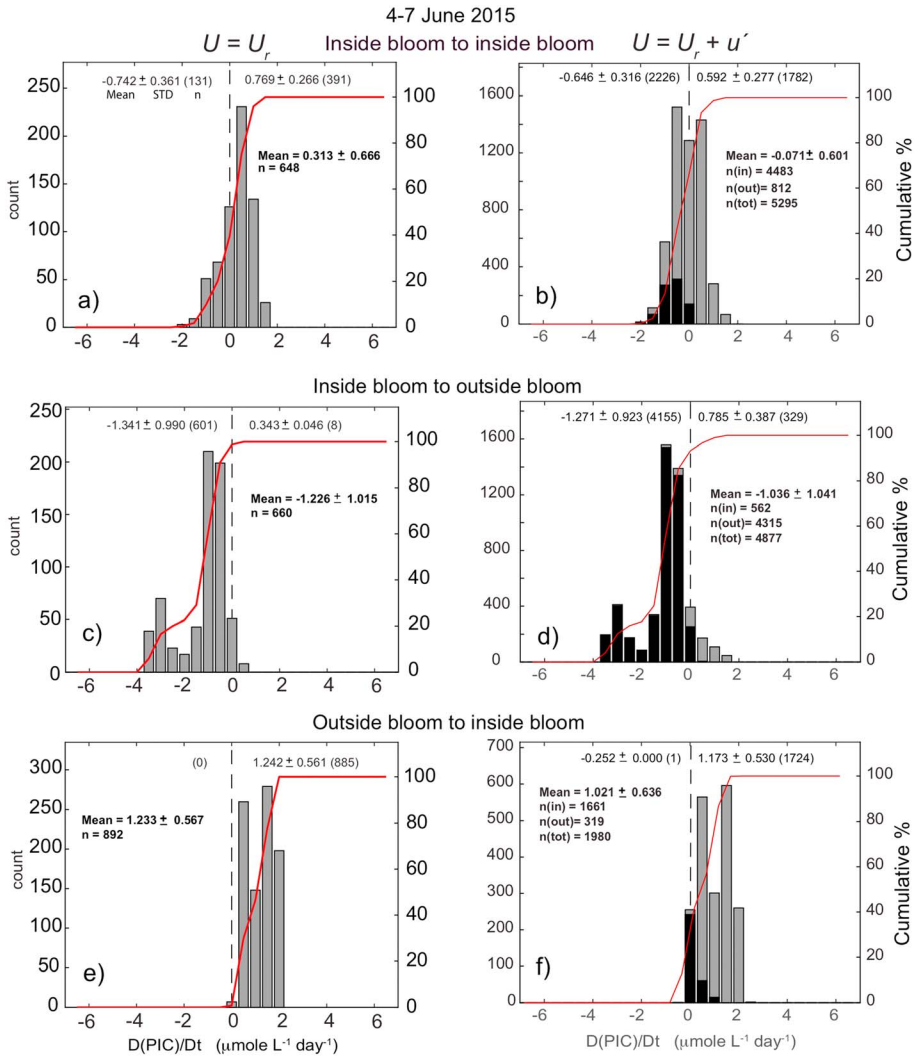

Figure 10. Histograms (stacked gray and black bars) and cumulative distributions (red lines) of D (PIC_{rs})/D*t* as defined in equation (4) for the 72-hr tracking period (4–7 June 2015). Histograms for trajectories starting and ending inside the bloom using (a) $\boldsymbol{U = U_r}$ or b) $\boldsymbol{U = U_r + u'}$ in 3. Histograms for trajectories starting inside and ending outside the bloom using (c) $\boldsymbol{U = U_r}$ or (d) $\boldsymbol{U = U_r + u'}$. Histograms for trajectories starting outside and ending inside the bloom using (e) $\boldsymbol{U = U_r}$ or (f) $\boldsymbol{U = U_r + u'}$. Black segments of histogram bars indicate trajectories that ended outside the bloom. Bold text indicates overall means, standard deviations, and total numbers inside and outside the bloom of D (PIC_{rs})/D*t* values. Means, standard deviations, and numbers of positive (negative) D (PIC_{rs})/D*t* values are shown in upper right (left) of each panel.

first and the second tracking periods was also found for trajectories computed with $\boldsymbol{U = U_r}$ that started outside and ended inside the bloom (Figures 9e and 10e): in the first tracking period D (PIC_{rs})/Dt ranged from about 0 to +6 µmol·L^{-1}·day^{-1} versus 0 to +2 µmol·L^{-1}·day^{-1} for the second.

For trajectories with $\boldsymbol{U = U_r}$ that started inside and ended outside the bloom (Figures 9c and 10c) the ranges in D (PIC_{rs})/D*t* were similar between tracking periods, −4 to 0 µmol·L^{-1}·day^{-1}, although the most frequently occurring D (PIC_{rs})/D*t* values were closer to zero in the second tracking period (Figures 9c and 9d vs. Figures 10c and 10d). Similarity of D (PIC_{rs})/D*t* distributions between Figures 9e and 9f, and between Figures 10e and 10f, indicated that D (PIC_{rs})/D*t* estimates were robust with respect to velocity uncertainty.

Distributions of D (PIC_{rs})/D*t* in the histograms of Figures 9 and 10 are consistent with our overall biological interpretation of a bloom growing during 2–4 June (tracking period 1) and senescing during 4–7 June (tracking period 2) as well as values from previous field studies. For example, they fall within the range

of gross calcification rates measured during an *E. huxleyi* bloom along the Patagonian Shelf (0.2 to 7.3 $\mu mol \cdot L^{-1} \cdot day^{-1}$) by Poulton et al. (2013). They are also consistent with a Lagrangian study in the North Sea where gross calcification rates within a water parcel tracked over six days ranged from 1.18 to 11.54 $\mu mol \cdot L^{-1} \cdot day^{-1}$ (Rees et al., 2002).

Our approach of estimating D (PIC_{rs})/Dt could lead to improved quantification of the $CaCO_3$ budget as this quantity can be obtained over wide areas of developing blooms. Furthermore, estimating rates of PIC production in the euphotic zone and its changes over bloom development with high temporal resolution and broad coverage will enable capturing transitions through bloom development associated with shifts in calcification. This is a critical step needed to reduce current uncertainties in the $CaCO_3$ budget (Iglesias-Rodriguez et al., 2002). An example of such a transition is suggested in our study by the differing D (PIC_{rs})/Dt distributions between the tracking periods. It is known that PIC production and particulate organic carbon (POC) production are decoupled during population development in *E. huxleyi*. Specifically, nutrient limitation appears to stimulate calcification (Berry et al., 2002; Riegman et al., 2000), resulting in an increase in PIC production with respect to POC (typically PIC:POC over 1 and up to 2.3), toward the end of blooms, in contrast with nutrient replete conditions, with PIC:POC generally below unity (Paasche, 2002). Also, at the end of blooms, populations have been shown to shift from calcifying vegetative cells to noncalcifying gametes bearing organic scales instead of coccoliths (Klaveness, 1972). Therefore, capturing different stages of calcification by observing changing D (PIC_{rs})/Dt during bloom development will likely be an important step in estimating regional calcium carbonate budgets.

4.4. Summary

This study reports on the first coastal *E. huxleyi* bloom known to have occurred along California. The bloom likely resulted from the rare cooccurrence of multiple environmental conditions (highly stratified water column, low inorganic nitrate, potentially elevated organic nitrogen following a widespread diatom bloom) during 2015. It is also the first study to track the population dynamics of a coastal coccolithophore bloom based on a combination of in situ observations of coccolithophore populations using flow cytometry, surface current data derived from HF radar, and satellite ocean color imagery. The use of D (PIC_{rs})/Dt allowed us to estimate how PIC production by this coastal coccolithophore bloom varied during bloom phases. Only a few other remote sensing studies have assessed the role of circulation on coccolithophore bloom dynamics such as those of Cokacar et al. (2001) and Balch et al. (2009). One study that used an approach somewhat similar to ours was that of Schofield et al. (2012) who determined that nearshore upwelling, rather than input from the Hudson River, was the nutrient source for a shelf-wide dinoflagellate bloom along the New Jersey coast, a conclusion based on ocean color satellite imagery and HF radar-derived trajectories.

Our approach of combining sequences of satellite ocean color images with HF radar-derived surface currents enabled us to retrospectively identify locations of developing bloom populations prior to satellite detection (e.g., green areas, Figures 7a and 8a). Such knowledge may help explain environmental characteristics that drive developing blooms. We speculate that this approach can be applied toward tracking development of harmful algae blooms, which occur seasonally in the SBC (Anderson et al., 2006; Anderson et al., 2016; Sekula-Wood et al., 2011), and in coastal regions worldwide where they threaten ecosystem health and food security (Anderson et al., 2002).

Acknowledgments
We thank Veronika Kivenson, Eleanor Arrington, Janice Jones, and Clint Nelson for assistance in collecting field samples. This work was supported by the National Science Foundation to M. D. I. R. (MRI-1337400) and by the Santa Barbara Coastal Long Term Ecological Research project (OCE 9982105, 0620276, and 1232779). P. G. M. was supported by the National Aeronautics and Space Administration, Biodiversity and Ecological Forecasting Program (Grant NNX14AR62A), the Bureau of Ocean Energy Management, Environmental Studies Program (BOEM Agreement MC15AC00006), and the National Oceanic and Atmospheric Administration (NOAA) in support of the Santa Barbara Channel Marine Biodiversity Observation Network. L. W. was supported by the National Science Foundation (OCE 1658475). D. A. S. and E. A. F. were funded by the NASA Ocean Biology and Biogeochemistry Program. Surface current data from HF radar and diatom abundance data were made available by the Southern California Coastal Ocean Observing System, a regional association of the NOAA Integrated Ocean Observing System (http://www.sccoos.org). Satellite remote sensing data were made available by the NASA Ocean Biology Processing Group (https://oceancolor.gsfc.nasa.gov/). All remaining data are contained within tables and figures.

References

Ackleson, S. G., Balch, W. M., & Holligan, P. M. (1994). Response of water-leaving radiance to particulate calcite and chlorophyll a concentrations: A model for the Gulf of Maine coccolithophore blooms. *Journal of Geophysical Research*, *99*, 1483–7499.

Anderson, C. R., Brzezinski, M. A., Washburn, L., & Kudela, R. (2006). Circulation and environmental conditions during a toxigenic *Pseudo-nitzchia australis* bloom in the Santa Barbara Channel, California. *Marine Ecology Progress Series*, *327*, 119–133. https://doi.org/10.3354/meps327119

Anderson, C. R., Kudela, R. M., Kahru, M., Chao, Y., Rosenfeld, L. K., Bahr, F. L., et al. (2016). Initial skill assessment of the California Harmful Algae Risk Mapping (C-HARM) system. *Harmful Algae*, *59*, 1–18. https://doi.org/10.1016/j.hal.2016.08.006

Anderson, D. M., Glibert, P. M., & Burkholder, J. M. (2002). Harmful algal blooms and eutrophication: Nutrient sources, composition, and consequences. *Estuaries*, *25*(4), 704–726. https://doi.org/10.1007/bf02804901

Balch, W. M., Gordon, H. R., Bowler, B. C., Drapeau, D. T., & Booth, E. S. (2005). Calcium carbonate measurements in the surface global ocean based on Moderate-Resolution Imaging Spectroradiometer data. *Journal of Geophysical Research*, *110*, C07001. https://doi.org/10.1029/2004JC002560

Balch, W. M., Holligan, P. M., Ackleson, S. G., & Voss, K. J. (1991). Biological and optical properties of mesoscale coccolithophore blooms in the Gulf of Maine. *Limnology and Oceanography*, *36*(4), 629–643. https://doi.org/10.4319/lo.1991.36.4.0629

Balch, W. M., Holligan, P. M., & Kilpatrick, K. A. (1992). Calcification, photosynthesis, and growth of the bloom-forming coccolithophore *Emiliania huxleyi*. *Continental Shelf Research*, *12*(12), 1353–1374. https://doi.org/10.1016/0278-4343(92)90059-s

Balch, W. M., Kilpatrick, K., Holligan, P. M., & Cucci, T. (1993). Coccolith production and detachment by *Emiliania huxleyi* (Prymnesiophyceae). *Journal of Phycology*, *29*(5), 566–575. https://doi.org/10.1111/j.0022-3646.1993.00566.x

Balch, W. M., Kilpatrick, K. A., Holligan, P., Harbour, D., & Fernandez, E. (1996). The 1991 coccolithophore bloom in the central North Atlantic Relating optics to coccolith concentration. *Limnology and Oceanography*, *41*(8), 1684–1696. https://doi.org/10.4319/lo.1996.41.8.1684

Balch, W. M., Plueddeman, A. J., Bowler, B. C., & Drapeau, D. T. (2009). Chalk-Ex-Fate of CaCO3 particles in the mixed layer: Evolution of patch optical properties. *Journal of Geophysical Research*, *114*, C07020. https://doi.org/10.1029/2008jc004902

Benner, I., & Passow, U. (2010). Utilization of organic nutrients by coccolithophores. *Marine Ecology Progress Series*, *404*, 21–29. https://doi.org/10.3354/meps08474

Berry, L., Taylor, A. R., Lucken, U., Ryan, K. P., & Brownlee, C. (2002). Calcification and inorganic carbon acquisition in coccolithophores. *Functional Plant Biology*, *29*, 289–299.

Bond, N. A., Cronin, M. F., Freeland, H., & Mantua, N. (2015). Causes and impacts of the 2014 warm anomaly in the NE Pacific. *Geophysical Research Letters*, *42*, 3414–3420. https://doi.org/10.1002/2015GL063306

Bratbak, G., Egge, J. K., & Heldal, M. (1993). Viral mortality of the marine alga *Emiliania huxleyi* (Haptophyceae) and termination of algal blooms. *Marine Ecology Progress Series*, *93*(1-2), 39–48. https://doi.org/10.3354/meps093039

Capet, X., McWilliams, J. C., Molemaker, M. J., & Shchepetkin, A. F. (2008). Mesoscale to Submesoscale Transition in the California Current System. Part II: Frontal Processes. *Journal of Physical Oceanography*, *38*(1), 44–64. https://doi.org/10.1175/2007JPO3672.1

Cokacar, T., Kubilay, N., & Oguz, T. (2001). Structure of *Emiliania huxleyi* blooms in the Black Sea surface waters as detected by SeaWIFS imagery. *Geophysical Research Letters*, *28*(24), 4607–4610. https://doi.org/10.1029/2001gl013770

Di Lorenzo, E., & Mantua, N. (2016). Multi-year persistence of the 2014/15 North Pacific marine heatwave. *Nature Climate Change*, *6*(11), 1042–1047. https://doi.org/10.1038/NCLIMATE3082

Emery, B. M., Washburn, L., & Harlan, J. A. (2004). Evaluating radial current measurements from CODAR high-frequency radars with moored current meters. *Journal of Atmospheric and Oceanic Technology*, *21*(8), 1259–1271. https://doi.org/10.1175/1520-0426(2004)021<1259:ERCMFC>2.0.CO;2

Emery, B. M., Washburn, L., Love, M. S., Hishimoto, M. M., & Ohlmann, J. C. (2006). Do oil and gas platforms off California reduce recruitment of bocaccio (Sebastes paucispinis) to natural habitat? An analysis based on trajectories derived from high-frequency radar. *Fishery Bulletin*, *104*, 391–400.

Eppley, R. W., Rogers, J. N., & McCarthy, J. J. (1969). Half saturation constant for uptake of nitrate and ammonium by marine phytoplankton. *Limnology and Oceanography*, *14*(6), 912–920. https://doi.org/10.4319/lo.1969.14.6.0912

Estapa, M. L., Siegel, D. A., Buesseler, K. O., Stanley, R. H., Lomas, M. W., & Nelson, N. B. (2015). Decoupling of net community and export production on submesoscales in the Sargasso Sea. *Global Biogeochemical Cycles*, *29*, 1266–1282. https://doi.org/10.1002/2014GB004913

Evans, C., Kadner, S. V., Darroch, L. J., Wilson, W. H., Liss, P. S., & Malin, G. (2007). The relative significance of viral lysis and microzooplankton grazing as pathways of dimethylsulfoniopropionate (DMSP) cleavage: An *Emiliania huxleyi* culture study. *Limnology and Oceanography*, *52*(3), 1036–1045. https://doi.org/10.4319/lo.2007.52.3.1036

Harms, S., & Winant, C. D. (1998). Characteristic patterns of the circulation in the Santa Barbara Channel. *Journal of Geophysical Reseach*, *103*(C2), 3041–3065. https://doi.org/10.1029/97JC02393

Heimdal, B. R., Egge, J. K., Veldhuis, M. J. W., & Westbroek, P. (1994). The 1992 Norwegian *Emiliania huxleyi* experiment. An overview. *Sarsia*, *79*(4), 285–290. https://doi.org/10.1080/00364827.1994.10413560

Henderikx Freitas, F., Siegel, D. A., Maritorena, S., & Fields, E. (2017). Satellite assessment of particulate matter and phytoplankton variations in the Santa Barbara Channel and its surrounding waters: Role of surface waves. *Journal of Geophysical Research: Oceans.*, *122*(1), 355–371. https://doi.org/10.1002/2016JC012152

Holligan, P. M., Groom, S. B., & Harbour, D. S. (1993). What controls the distribution of the coccolithophore, *Emiliania huxleyi*, in the North Sea? *Fisheries Oceanography*, *2*(3-4), 175–183. https://doi.org/10.1111/j.1365-2419.1993.tb00133.x

Holligan, P. M., Viollier, M., Harbour, D. S., Camus, P., & Champagne-Philippe, M. (1983). Satellite and ship studies of coccolithophore production along a continental shelf edge. *Nature*, *304*(5924), 339–342. https://doi.org/10.1038/304339a0

Iglesias-Rodriguez, M. D., Armstrong, R., Feely, R., Hood, R., Kleypas, J., Milliman, J. D., et al. (2002). Progress made in study of ocean's calcium carbonate budget. *Eos Trans. Am. Geophys. Union*, *83*(34), 365–375. https://doi.org/10.1029/2002EO000267

Jönsson, B. F., & Salisbury, J. E. (2016). Episodicity in phytoplankton dynamics in a coastal region. *Geophysical Research Letters*, *43*, 5821–5828. https://doi.org/10.1002/2016GL068683

Jönsson, B. F., Salisbury, J. E., & Mahadevan, A. (2009). Extending the use and interpretation of ocean satellite data using Lagrangian modeling. *International Journal of Remote Sensing*, *30*(13), 3331–3341. https://doi.org/10.1080/01431160802558758

Jönsson, B. F., Salisbury, J. E., & Mahadevan, A. (2011). Large variability in continental shelf production of phytoplankton carbon revealed by satellite. *Biogeosciences*, *8*(5), 1213–1223. https://doi.org/10.5194/bg-8-1213-2011

Klaveness, D. (1972). *Coccolithus huxleyi* (Lohm.) Kamptn. II. The flagellate cell, aberrant cell types, vegetative propagation and life cycles. *British Phycological Journal*, *7*(3), 309–318. https://doi.org/10.1080/00071617200650321

Krumhardt, K. M., Lovenduski, N. S., Iglesias-Rodriguez, M. D., & Kleypas, J. A. (2017). Coccolithophore growth and calcification in a changing ocean. *Progress in Oceanography*, *159*, 276–295. https://doi.org/10.1016/j.pocean.2017.10.007

Leising, A. W., Schroeder, I. D., Bograd, S. J., Abell, J., Durazo, R., Gaxiola-Castro, G., et al. (2015). State of the California Current 2014-15: impacts of the warm-water "blob". *California Cooperative Oceanic Fisheries Investigations Reports*, *56*, 31–68.

McCabe, R. M., Hickey, B. M., Kudela, R. M., Lefebvre, K. A., Adams, N. G., Bill, B. D., & Trainer, V. L. (2016). An unprecedented coastwide toxic algal bloom linked to anomalous ocean conditions. *Geophysical Research Letters*, *43*, 10,366–310,376. https://doi.org/10.1002/2016GL070023

McClatchie, S., Goericke, R., Leising, A. W., Auth, T., Bjorkstedt, E. P., Robertson, R. R., and C. A. Morgan (2016). State of the California Current 2015-16: comparisons with the 1997-98 El Niño. California Cooperative Oceanic Fisheries Investigations Reports, 57, 5-61.

Moore, T. S., Dowell, M. D., & Franz, B. A. (2012). Detection of coccolithophore blooms in ocean color satellite imagery: A generalized approach for use with multiple sensors. *Remote Sensing of Environment*, *117*, 249–263. https://doi.org/10.1016/j.rse.2011.10.001

Morel, A., Gentili, B., Claustre, H., Babin, M., Bricaud, A., Ras, J., & Tièche, F. (2007). Optical properties of the "clearest" natural waters. *Limnology and Oceanography*, *52*(1), 217–229. https://doi.org/10.4319/lo.2007.52.1.0217

Müller, M., Antia, A., & Laroche, J. (2008). Influence of cell cycle phase on calcification in the coccolithophore *Emiliania huxleyi*. *Limnology and Oceanography*, *53*(2), 506–512. https://doi.org/10.4319/lo.2008.53.2.0506

Nanninga, H. J., & Tyrrell, T. (1996). Importance of light for the formation of algal blooms by *Emiliania huxleyi*. *Marine Ecology Progress Series*, *136*, 195–203. https://doi.org/10.3354/meps136195

Neukermans, G., Oziel, L., & Babin, M. (2018). Increased intrusion of warming Atlantic water leads to rapid expansion of temperate phytoplankton in the Arctic. *Global Change Biology.*, *24*, 2545–2553. https://doi.org/10.1111/gcb.14075

Ohlmann, J. C., LaCasce, J. H., Washburn, L., Mariano, A. J., & Emery, B. (2012). Relative dispersion observations and trajectory modeling in the Santa Barbara Channel. *Journal of Geophysical Research*, *117*, C05040. https://doi.org/10.1029/2011JC007810

Paasche, E. (2002). A review of the coccolithophorid *Emiliania huxleyi* (Prymnesiophyceae), with particular reference to growth, coccolith formation, and calcification–photosynthesis interactions. *Phycologia*, *40*, 503–529.

Poulton, A. J., Painter, S. C., Young, J. R., Bates, N. R., Bowler, B., Drapeau, D., et al. (2013). The 2008 *Emiliania huxleyi* bloom along the Patagonian Shelf: Ecology, biogeochemistry, and cellular calcification. *Global Biogeochem Cycles*, *27*, 1023–1033. https://doi.org/10.1002/2013GB004641

Reed, D., Washburn, L., Rassweiler, A., Miller, R., Bell, T., & Harrer, S. (2016). Extreme warming challenges sentinel status of kelp forests as indicators of climate change. *Nature Communications*, *7*(1). https://doi.org/10.1038/ncomms13757

Rees, A. P., Malcolm, E., Woodward, S., Robinson, C., Cummings, D. G., Tarran, G. A., & Joint, I. (2002). Size-fractionated nitrogen uptake and carbon fixation during a developing coccolithophore bloom in the North Sea during June 1999. *Deep-Sea Research II*, *49*(15), 2905–2927. https://doi.org/10.1016/S0967-0645(02)00063-2

Riegman, R., Stolte, W., Noordeloos, A. A. M., & Slezak, D. (2000). Nutrient uptake and alkaline phosphatase (EC3:1:3:1) activity of *Emiliania huxleyi* (Prymnesiophyceae) during growth under N and P limitation in continuous cultures. *Journal of Phycology*, *36*(1), 87–96. https://doi.org/10.1046/j.1529-8817.2000.99023.x

Rivero-Calle, S., Gnanadesikan, A., Del Castillo, C. E., Balch, W., & Guikema, S. D. (2015). Multidecadal increase in North Atlantic coccolithophores and the potential role of rising CO2. *Science*, *350*(6267), 1533–1537. https://doi.org/10.1126/science.aaa8026

Rowe, M. D., Anderson, E. J., Wynne, T. T., Stumpf, R. P., Fanslow, D. L., Kijanka, K., & Davis, T. W. (2016). Vertical distribution of buoyant Microcystis blooms in a Lagrangian particle tracking model for short-term forecasts in Lake Erie. *Journal of Geophysical Research: Oceans*, *121*, 5296–5314. https://doi.org/10.1002/2016JC011720

Schofield, O., H. Roarty, G. Saba, X. Yi, J. Kohut, S. Glenn, et al. (2012) Phytoplankton dynamics and bottom water oxygen during a large bloom in the summer of 2011, Oceans 2012 MTS/IEEE: Harnessing the Power of the Ocean. DOI: https://doi.org/10.1109/OCEANS.2012.6405078

Sekula-Wood, E., Benitez-Nelson, C., Morton, S., Anderson, C., Burrell, C., & Thunell, R. (2011). *Pseudo-nitzschia* and domoic acid fluxes in Santa Barbara Basin (CA) from 1993 to 2008. *Harmful Algae*, *10*(6), 567–575. https://doi.org/10.1016/j.hal.2011.04.009

Sieracki, M. E., Verity, P. G., & Stoecker, D. K. (1993). Plankton community response to sequential silicate and nitrate depletion during the 1989 North Atlantic spring bloom. *Deep-Sea Res II*, *40*(1-2), 213–225. https://doi.org/10.1016/0967-0645(93)90014-E

Smayda, T. J. (1989). Primary production and the global epidemic of phytoplankton blooms in the sea: a linkage? In E. M. Cosper, V. M. Bricelj, & E. J. Carpenter (Eds.), *Novel phytoplankton blooms*, (pp. 449–483). Verlag, Berlin: Springer. https://doi.org/10.1007/978-3-642-75280-3_26

Tyrrell, T., & Merico, A. (2004). *Emiliania huxleyi: bloom observations and the conditions that induce them*. Berlin: Springer-Verlag Berlin.

Ullman, D. S., O'Donnell, J., Kohut, J., Fake, T., & Allen, A. (2006). Trajectory prediction using HF radar surface currents: Monte Carlo simulations of prediction uncertainties. *Journal of Geophysical Research*, *111*, C12005. https://doi.org/10.1029/2006JC003715

Venrick, E. L. (2002). Floral patterns in the California Current System off southern California: 1990-1996. *Journal of Marine Research*, *60*(1), 171–189. https://doi.org/10.1357/002224002762341294

Venrick, E. L. (2015). Phytoplankton species in the California Current system off Southern California: the spatial dimensions. California Cooperative Oceanic Fisheries Investigations Reports, *56*, 168-184.

Winter, A. (1985). Distributio of living coccolithophores in the California Current system, southern California borderland. *Marine Micropaleontology*, *9*(5), 385–393. https://doi.org/10.1016/0377-8398(85)90007-6

Wynne, T. T., Stumpf, R. P., Tomlinson, M. C., Fahnenstiel, G. L., Dyble, J., Schwab, D. J., & Joshi, S. J. (2013). Evolution of a cyanobacterial bloom forecast system in western Lake Erie: Development and initial evaluation. *Journal of Great Lakes Research*, *39*, 90–99. https://doi.org/10.1016/j.jglr.2012.10.003

Wynne, T. T., Stumpf, R. P., Tomlinson, M. C., Schwab, D. J., Watabayashi, G. Y., & Christensen, J. D. (2011). Estimating cyanobacterial bloom transport by coupling remotely sensed imagery and a hydrodynamic model. *Ecological Applications*, *21*(7), 2709–2721. https://doi.org/10.1890/10-1454.1

Ziveri, P., Thunell, R. C., & Rio, D. (1995). Seasonal changes in coccolithophore densities in the Southern California Bight during 1991–1992. *Deep Sea Research Part I: Oceanographic Research Papers*, *42*(11–12), 1881–1903. https://doi.org/10.1016/0967-0637(95)00089-5

Zondervan, I. (2007). The effects of light, macronutrients, trace metals and CO_2 on the production of calcium carbonate and organic carbon in coccolithophores—A review. *Deep Sea Res II*, *54*(5-7), 521–537. https://doi.org/10.1016/j.dsr2.2006.12.004